



PCCP

Emergent ultras-small multiferroics in paraelectric perovskite oxide by hole polarons

Journal:	<i>Physical Chemistry Chemical Physics</i>
Manuscript ID	CP-ART-11-2023-005364.R1
Article Type:	Paper
Date Submitted by the Author:	29-Nov-2023
Complete List of Authors:	Xu, Tao; Kyoto University Mori, Masataka; Kyoto University Hirakata, Hiroyuki; Kyoto University, Department of Mechanical Engineering and Science Kitamura, Takayuki; Kyoto University Shimada, Takahiro; Kyoto University, Department of Mechanical Engineering and Science

SCHOLARONE™
Manuscripts

Emergent ultrasmall multiferroics in paraelectric perovskite oxide by hole polarons

Tao Xu*, Masataka Mori, Hiroyuki Hirakata, Takayuki Kitamura, Takahiro Shimada**

Department of Mechanical Engineering and Science, Kyoto University, Nishikyo-ku, Kyoto 615-8540, Japan

ABSTRACT

Ultimately small multiferroics with coupled ferroelectric and ferromagnetic order parameters have drawn considerable attention for their tremendous technological potential. Nevertheless, these ferroic orders inevitably disappear below the critical size of several nanometers in conventional ferroelectrics or multiferroics. Here, based on first-principles calculations, we propose a new strategy to overcome this limitation and create ultrasmall multiferroic elements in otherwise nonferroelectric CaTiO_3 by engineering the interplay of oxygen octahedral rotations and hole polarons, though both of them are generally believed to be detrimental to ferroelectricity. It is found that the hole doped in CaTiO_3 spontaneously forms a localized polaronic state. The lattice distortions associated with a hole polaron interacting with the intrinsic oxygen octahedral rotations in CaTiO_3 effectively break the inversion symmetry and create atomic-scale ferroelectricity beyond the critical size limitation. The hole polaron also causes highly localized magnetism attributed to the associated spin-polarized electric state and thus manifests as a multiferroic polaron. Moreover, the hole polaron exhibits high hopping mobility accompanied by rich switching of polarization and magnetic directions, indicating strong magnetoelectric coupling with a mechanism dissimilar from that of conventional multiferroics. The present work provides a new mechanism to engineer inversion symmetry and opens avenues for designing unusual multifunctional materials.

1. Introduction

Magnetoelectric multiferroics, in which ferroelectricity and ferromagnetism coexist [1,2], have attracted large amounts of attention owing to the fascinating physical properties arising from the coupling of different ferroic orders as well as their significant application prospects in advanced technological devices such as multiple-state memories and magnetoelectric sensors [3, 4]. While remarkable successes have been obtained in exploring multiferroics with excellent performance [5-8], achieving nanoscale multiferroic properties is still urgent and vital to meet the growing demand for miniaturized, integrated electronic devices. However, retaining the stability of multiferroic orders at the nanoscale is challenging due to depolarization field and surface effects that suppress or destabilize the ferroic orders completely below the critical size [9-11]. For example, ferroelectric PZT and BaTiO₃ nanodots have been reported to lose ferroelectricity with sizes below 3–5 nm [12,13]. Although great efforts have recently been devoted to exploring multiferroics at even smaller sizes under strict conditions, the magnitude of ferroic orders has also progressively decreased. Therefore, there is an inevitable physical limit for ferroic properties and the direct scale-down of conventional multiferroics to ultimately small size cannot be achieved in principle.

Oxygen octahedral rotation is one of the fundamental atomic distortions in perovskite oxides and has a dramatic impact on electronic and magnetic behaviors. Although the oxygen octahedral rotation tends to compete with and suppress ferroelectric distortions in common perovskites, such as SrTiO₃ and CaTiO₃, engineering oxygen octahedral rotations in perovskites has emerged as a powerful route to discover and design exotic electronic phenomena and new functionalities. For example, octahedral rotation-driven ferroelectricity [14,15] and even strong polarization-magnetization coupling [16] have been predicted theoretically and observed experimentally. Octahedral rotations have also been

exploited to control the metal-insulator transitions and magnetic states [17,18]. These discoveries inspire the exploration of novel mechanisms mediated by oxygen octahedral rotations in pursuit of state-of-art atomic-scale multiferroics, even in intrinsically nonmagnetic and paraelectric CaTiO_3 compounds. On the other hand, excess charge carriers (electrons or holes) are pervasive in perovskite oxides [19-23] due to lattice defects in specific chemical environments or can be intentionally generated by applying high voltages and irradiation. One of the most fascinating manifestations of the electron configuration in perovskites is the highly localized polaronic state [24-26], which has been proven to offer a wide range of extraordinary functionalities and unusual coexisting properties that are inaccessible in host materials. Specifically, when polarons are formed, local mismatch in charge balance occurs, and nearby atoms are displaced, leading to the formation of characteristic atomic and electronic structures around the polaronic site. Due to the strong electron-lattice correlations, it is, in principle, possible to tailor the oxygen octahedral rotations and the resulting functionalities by charge carrier engineering [27].

In this work, we propose a new strategy to engineer oxygen octahedral rotation through hole localization, which unexpectedly breaks the inversion symmetry of centrosymmetric CaTiO_3 and creates electric polarization within the two-unit-cell region. The localized hole polaron is in a spin-polarized state and induces atomic-scale multiferroics in CaTiO_3 . Furthermore, we investigated the dynamics of the hole polaron and discussed the associated magnetoelectric coupling.

2. Methods

First-principles calculations were carried out in the framework of density functional theory using a plane-wave basis set with an energy cutoff of 500 eV, as implemented in the VASP [28,29]. The

projector-augmented wave (PAW) pseudopotential method [30,31] was utilized, and the 3s, 3p and 4s electrons for Ca, the 3s, 3p, 3d and 4s electrons for Ti, and the 2s and 2p electrons for O were treated as the valence states. The Monkhorst-Pack k -point mesh of $2 \times 2 \times 3$ was chosen for the Brillouin zone integration. In all calculations, the energy and force convergences criteria were set to 1.0×10^{-6} eV/cell and 0.01 eV/Å, respectively. The effect of spin polarization was included in the calculations, and fully unconstrained noncollinear magnetic calculations including the effect of spin-orbital coupling [32] were performed to obtain the magnetic anisotropy energy. The exchange-correlation energies were represented by the HSE06 hybrid-functional method [33,34], which can accurately describe the electronic structures of various semiconductors and was necessary for the calculation of the present polaronic state in CaTiO₃.

The crystal structure of perovskite oxide CaTiO₃ is a nonpolar paraelectric phase characterized by intrinsic antiferrodistortive distortions with a nonpolar $Pnma$ space group, as illustrated in Fig. S1. The red dot box indicates the primitive cell, which contains four formula units of CaTiO₃ with twenty atoms. The antiferrodistortive distortions consist of two kinds of TiO₆ octahedral rotations: two out-of-phase tilts along the [100] and [010] directions and one in-phase tilt along the [001] direction. This is in accordance with the orthorhombic $a^-a^+c^+$ Glazer system [35]. Owing to the symmetry breaking of the oxygen octahedral rotations, there are two kinds of inequivalent oxygen atoms, denoted O1 and O2 in Fig. S1, which are located within the (001) CaO and (001) TiO₂ planes, respectively. The lattice parameters obtained from HSE06 are $a = 5.36$ Å, $b = 5.43$ Å, and $c = 7.61$ Å, which reasonably agrees with the experimental data (see Table S1) [36,37]. Figure 1 illustrates the simulation supercell of the hole-doped CaTiO₃ system constructed from the primitive cell. The supercell contains 16 formula units with 80 atoms, and the dimensions are $|\mathbf{a}_1| = 2a$, $|\mathbf{a}_2| = 2b$, $|\mathbf{a}_3| = c$. A hole is created by removing an

electron from the calculated supercell with the same amount of homogeneous negative background charges, corresponding to a density of 0.0625 e /unit cell. This value is within the experimentally obtained hole density of 0.00 ~ 0.08 e /unit cell in perovskite oxides [38]. The hole polaron is obtained by introducing a precursor potential for polaron trapping by applying a small perturbation around a selected octahedral TiO_6 followed by full geometry optimization.

3. Results and discussions

3.1 Hole polaron

We started by probing the stable configurations of the excess hole in CaTiO_3 by calculating the formation energy E_{form} of the hole polaron, defined as $E_{\text{form}} = E_{\text{p}} - E_{\text{f}}$. Here, E_{p} and E_{f} are the energies of the polaronic and free-carrier states, respectively. The obtained values for the O1 and O2 atoms are -292 meV and -328 meV, respectively, indicating that the energetic favor of the polaronic states with respect to their delocalized counterparts and O2-polaron is the most stable configuration. The electronic density of states of the most stable O2-polaron was investigated, and the results are shown in Fig. 2(a), in which the valence band maximum (VBM) is set at the zero energy level. The conduction band minimum (CBM) appears at 3.8 eV above the edge of the valence band and is consistent with previous results without electron holes. Furthermore, an unoccupied electronic state appears within the bandgap that is absent in perfect CaTiO_3 . Thus, this is the defect state introduced by the excess hole. The single in-gap defect state is located 1.3 eV above the VBM, which is distinct from those of delocalized holes with metallic conductivity characteristics [39] and is evidence of the hole polaron. The spatial distribution of the squared wave function $|\psi_{\text{e}}|^2$ of the hole is shown in Fig. 2(b). The hole polaron is evidently trapped at one O2 site exhibiting $2p_y$ and $2p_z$ orbital characteristics and is

coherently coupled to local lattice distortions. Therefore, a hole in CaTiO_3 tends to be in a self-trapped state at O2 atoms in the form of a small polaron.

3.2 Ferroelectric polarization

The formation of a hole polaron is associated with significant local lattice distortions. As illustrated in Fig. 2(c), for the distribution of atomic displacements, the center O anion accommodating the hole polaron and the neighboring Ca cation and two Ti cations display large displacements relative to the paraelectric structure. In particular, O^{2-} and Ca^{2+} possess opposite displacements along the $[0\ 1\ 1]$ and $[0\bar{1}\bar{1}]$ directions, respectively, resulting in the separation of the centers of the positive and negative charges in the local unit cell from the original centrosymmetric structure. Since ferroelectricity arises from the relative displacements between the cation and anion, such large off-centered displacements are expected to induce local dipole moments in the otherwise paraelectric CaTiO_3 . The magnitude of such polarization is indeed verified by the modern theory of polarization using standard Berry phase calculations. We take the centrosymmetric structure as a reference and obtain a nontrivial total spontaneous polarization of $\mathbf{P}_{\text{tot}} = (0.13, 1.50, 1.31) \mu\text{C}/\text{cm}^2$, which is along the direction close to $[0\bar{1}\bar{1}]$.

The local polarization distribution of the unit cells around the hole polaron is further analyzed by utilizing the Born effective charge. The obtained results are illustrated in Fig. 3(a), in which the yellow arrows denote the local polarization within a unit cell. The effect of the hole polaron is almost confined to a $2 \times 1 \times 1$ unit-cell region around the polaron (denoted by the white dotted lines), while those beyond this region display negligible local polarization. The obtained average polarization of these local polarizations is denoted by the white arrow, which is nonzero and lies along the $[0\bar{1}\bar{1}]$ direction. This

is consistent with the Berry phase approach for evaluating ferroelectricity, indicating that the hole-induced ferroelectricity is confined to a two-unit-cell length.

To elucidate the mechanism of the emergent electric polarization in the otherwise non-ferroelectric CaTiO_3 , the atomic displacements specific to CaTiO_3 with hole polarons are analyzed in detail. The schematic diagram of perovskite CaTiO_3 with uniaxial oxygen octahedral rotation is shown in Fig. S2. For simplicity, it is shown from the axial top view, in which the oxygen atoms shift off the ideal face-centered position. This leads to local relative displacements between cations and anions, i.e., O atoms approach one side of the Ca atoms while moving away from the other. However, this displacement pattern is centrosymmetric, and their sum equals zero macroscopically, contributing to zero macroscopic polarization in CaTiO_3 . Due to the formation of a hole polaron, on the other hand, the approach of Ca and O atoms generates a robust repulsive ionic interaction between the cation Ca and the O that accommodate the hole polaron, resulting in additional relative displacement between them, i.e., off-center displacement with respect to the centrosymmetric antiferrodistortive configuration, with a structural change from $Pnma$ to Pm space group symmetry. This considerable off-center displacement results in the separation of the centers of the negative and positive charges in the local unit cell and enables each O₂-polaron to act as a polar element with a dipole moment in the same direction as that of O displacement in the oxygen octahedral rotations. In practice, perovskite CaTiO_3 has the $a^-a^+c^+$ oxygen octahedral rotation pattern [40], which induces the atomic displacement of O atoms along the $[0\bar{1}\bar{1}]$ direction and will induce $[0\bar{1}\bar{1}]$ direction electric polarization once hole polaron is formed based on the above discussions. This is consistent with the results from the Berry phase approach. Therefore, the hole polaron in CaTiO_3 displays atomic-scale ferroelectricity due to the interaction of oxygen octahedral rotations and the local symmetry breaking associated with the

polaron.

3.3 Magnetic properties and multiferroics

In addition to the electric polarization, we further explored the effect of hole polarons on the magnetic properties of CaTiO_3 . A nontrivial total magnetic moment of $1.0 \mu_B$ appears unexpectedly in the hole polaron system, even though CaTiO_3 is intrinsically nonmagnetic. As visualized in Fig. 3(b) for the detailed magnetization density distribution, the magnetization is mainly localized at the center O atom, consistent with the charge density distribution of the hole polaron as discussed above. This highly confined magnetism originates from the localized polaronic electronic state in the bandgap, which changes the normal O^{2-} to O^{1-} and creates spin-polarized electronic states, as discussed regarding the electronic density. We further calculate the magnetic anisotropy energy (MAE), defined as the energy difference between the magnetism aligned along the easy axis (or plane) and the hard axis (or plane). The obtained magnetocrystalline anisotropy energy surface of the hole polaron is depicted in the right panel of Fig. 3(b). It is found that the hole polaron exhibits obvious magnetic anisotropy with the easy axis lying along $[100]$, which is the perpendicular direction with respect to the CaO plane that accommodates the hole polaron. In addition, the computed MAE is $E_{[100]} - E_{(100)} = 2.5 \mu \text{eV}$. This value is nontrivial and even slightly larger than the value of $1.4 \mu\text{eV}/\text{atom}$ of Fe (bcc). The large MAE suggests strong magnetoelectric coupling in the systems, as will be discussed later.

The above results thus demonstrate a novel route for creating ultrasmall multiferroic elements beyond the critical size limit of intrinsic multiferroics, even in nonmagnetic paraelectric materials. Although CaTiO_3 is intrinsically nonmagnetic paraelectric, the spontaneous formation of a hole polaron induces the coexistence of ferroelectricity and magnetism, which are closely confined within

a two-unit-cell length region (i.e., approximately 8 Å). This atomic-scale multiferroic element is unavailable in conventional multiferroics, as the depolarization field and surface effects suppress it. Therefore, the charge carriers in *p*-type semiconductors, i.e., electron holes, spontaneously form hole polarons and act as ultrascale multiferroic elements.

3.4 Mobility of hole polarons

It is well established that a polaron is a quasiparticle consisting of a charge carrier and associated phonons or lattice deformation, which can move to adjacent sites through lattice vibration. To understand the dynamics of the multiferroic polaron, we further investigate the mobility of hole polarons, which can be approximated by the following equation:

$$\mu = [ea^2\omega_0/k_B T][\exp(-E_a/k_B T)] \quad (1)$$

where e is an elementary charge, a is the hopping distance between two neighboring O atoms, ω_0 is the frequency of the longitudinal optical phonon, k_B is Boltzmann's constant, and E_a is the activation barrier for hole polaron hopping between two neighboring O sites. The activation energy is estimated by linearly interpolating two polaron configurations [41, 42] (see Fig. S3). We consider the hopping of hole polaron between different O2 sites along various pathways, as illustrated in Fig. 4. The migration within the (001) plane involves hopping between equivalent O2 sites (i.e., O2-b ~ O2-e), while migration in the [001] direction proceeds via the less stable O1 sites (i.e., O1-a ~ O1-d). Figure 4(b) shows the calculated energy profiles for all the polaron migration pathways within the (001) plane. The lowest energy pathway is between O2-a and O2-b/O2-d with an activation energy of 148.0 meV. Taking $E_a = 148.0$ meV, $a = 2.772$ Å, $\omega_0 = 2.596 \times 10^{13}$ Hz [43], and $k_B = 1.381 \times 10^{-23}$ m²kg/(s²K), we obtain $\mu = 2.52 \times 10^{-3}$ cm²/Vs at room temperature, which is several orders larger than the

corresponding speed of oxygen vacancy in oxides ($10^{-8} \sim 10^{-6} \text{ cm}^2/\text{Vs}$) [44]. We also obtain a comparable μ of $1.19 \times 10^{-3} \text{ cm}^2/\text{Vs}$ for the migration between O2-a and O2-c/O2-e using the same method, indicating the feasibility of these pathways within the plane. In addition, the energy variations for polaron hopping among the O2 sites along the [001] direction via less stable O1 sites are shown in Fig. 4(c), and they exhibit energy barriers in the range of 136.9–265.5 meV. The corresponding polaron mobility μ associated with these four hopping paths is also calculated, and all these results are summarized in Table S2. It is evident that hopping between the more stable O2 site and the stable O1-a and O1-d sites is also possible due to their high mobility. Thus, the hole polaron in CaTiO_3 has high mobility and easily migrates to neighboring oxygen sites.

3.5 Switching of hole polarons

In addition, ferroelectric and magnetic switching is vital in the utilization of multiferroics. Based on the above results, we discuss the dynamic switching characteristics of hole polarons. The O2 atoms in the primitive cell of CaTiO_3 are highlighted in Fig. S4, and the corresponding directions of polarization and magnetic moments are summarized in Table 1. For instance, for the polaron localized on the O2-p1 site, the polarization and magnetism are along $[0\bar{1}\bar{1}]$ and $[100]$, while the corresponding directions turn to $[\bar{1}01]$ and $[010]$, respectively, when the polaron migrates to the O2-p2 site. This site-dependent multiferroic direction originates from the relative displacements of oxygen octahedral rotations, as discussed above. Due to the high hopping mobility of hole polarons among O2 atoms, the ferroelectric and magnetic moment directions can thus be switched dynamically. These site-dependent multiferroic directions indicate that multiferroics can be switched in eight different directions through the migration of hole polarons among these O2 sites. Therefore, in contrast to the conventional multiferroic

switching mechanism, the high mobility of hole polarons and the resulting movement of atomic-scale multiferroic elements achieve the switching process. Finally, the magnetoelectric coupling is also evident in the system from Table 1 and Fig. S4(b): the initial [100] magnetism (hole polaron on the O2-p1 site) tends to switch to the [010] direction by means of an [010] external magnetic field; due to the high mobility, the polaron will easily hop to the O2-p2 site with the preferred direction of the magnetic moment, resulting in switching of the direction of electric polarization (i.e., from $[0\bar{1}\bar{1}]$ to $[\bar{1}01]$). Similarly, we can also obtain the response of magnetism by applying an electric field. Therefore, the spontaneous localization of holes in CaTiO_3 and its high hopping mobility manifests as an atomic-scale multiferroic element with magnetoelectric coupling, breaking the intrinsic size limitations for conventional multiferroics.

4. Conclusion

In summary, we propose a strategy that effectively exploits the interaction of hole polarons with the intrinsic oxygen octahedral rotations in CaTiO_3 to create atomic-scale ferroelectricity beyond the critical size limitation. Our first-principles calculations established that the electron hole spontaneously forms a localized polaronic state and induces localized ferroelectric polarization due to local symmetry breaking. We also show that the hole polaron carries highly localized magnetism and manifests as an ultrasmall multiferroic element. Finally, we demonstrate the high mobility of the hole polaron owing to its low activation energy of polaron hopping and discuss the associated magnetoelectric coupling. These results demonstrate that the modification of oxygen octahedral rotations through hole polarons offers a new route to create extraordinary functionalities in perovskite materials.

Corresponding Authors

*E-mail: xu.tao.44a@st.kyoto-u.ac.jp;

**E-mail: shimada@me.kyoto-u.ac.jp

Acknowledgment

This work was supported by JSPS KAKENHI (Grant Numbers JP23H00159, JP23K17720, JP20H05653) and JST FOREST Program (Grant Number JPMJFR222H) and JSPS International Research Fellow (No. P22065).

Reference

- [1] W. Eerenstein, N. D. Mathur, J. F. Scott, *Nature (London)*, 2006, **442**, 759765.
- [2] N. A. Spaldin, R. Ramesh, *Nat. Mater.*, 2019, **18**, 203212.
- [3] H. Béa, M. Gajek, M. Bibes, A. Barthélémy, *J. Phys. Condens. Matter.*, 2008, **20**, 434221.
- [4] X. L. Liu, D. Li, H. X. Zhao, X. Dong and L. Zheng, *Adv. Mater.*, 2021, **33**, 2004542.
- [5] Y. Ba, S. H. Zhuang, Y. K. Zhang, Y. T. Wang, Y. Gao, H. G. Zhou, M. F. Chen, W. D. Sun, Q. Liu, G. Z. Chai, *Nat. Commun.*, 2021, **12**, 322.
- [6] N. A. Spaldin, R. Ramesh, *Nat. Mater.*, 2019, **18**, 203212.
- [7] Xu, T. , Shimada, T. , Araki, Y. , Wang, J. , & Kitamura, T., *Nano Letters*, 2016, **16**, 454–458.
- [8] Bagri, A., Phase, D.M., Choudhary, R. J., *Acta Materialia*, 2023, **255**, 119091.
- [9] J. Junquera, P. Ghosez, *Nature (London)*, 2003, **422**, 506509.
- [10] D. D. Fong, G. B. Stephenson, S. K. Streiffer, J. A. Eastman, O. Auciello, P. H. Fuoss, C. Thompson, *Science*, 2004, **304** 16501653.
- [11] L. Despont, C. Koitzsch, F. Clerc, M. G. Garnier, P. Aebi, C. Lichtensteiger, J. M. Triscone, F. J. G. D. Abajo, E. Bousquet, P. Ghosez, *Phys. Rev. B*, 2006, **73**, 094110.
- [12] I. I. Naumov, L. Bellaiche, H. X. Fu, *Nature (London)*, 2004, **432**, 737740.
- [13] M. J. Polking, M. G. Han, A. Yourdkhani, V. Petkov, C. F. Kisielowski, V. V. Volkov, Y. Zhu, G. Caruntu, a P. Alivisatos, R. Ramesh, *Nat. Mater.*, 2012, **11**, 700.
- [14] E. Bousquet, M. Dawber, N. Stucki, C. Lichtensteiger, P. Hermet, S. Gariglio, J. M. Triscone, P. Ghosez, *Nature (London)*, 2008, **452**, 732736.
- [15] J. M. Rondinelli, C. Fennie, *Adv. Mater.*, 2012, **24**, 19611968.
- [16] N. A. Benedek, C. Fennie, *Phys. Rev. Lett.* 2011, **106**, 107204.
- [17] B. Chen, N. Gauquelin, R. J. Green, J. H. Lee, C. Piamonteze, M. Spreitzer, D. Jannis, J. Verbeeck, M. Bibes, M. Huijben, *Nano. Lett.* 2021, **21**, 12951302.
- [18] H. Akamatsu, Y. Kumagai, F. Oba, K. Fujita, K. Tanaka, and I. Tanaka, *Adv. Funct. Mater.*, 2013, **23**, 1864.
- [19] A. Q. Jiang, Y. Y. Lin, T. A. Tang, *J. Appl. Phys.*, 2007, **102**, 074109.
- [20] H. Du, X. Lin, Z. M. Xu, D. W. Chu, *J. Mater. Sci.*, 2015, **50**, 56415673.
- [21] T. Shimada, T. Xu, Y. Araki, J. Wang, T. Kitamura, *Nano. Lett.*, 2017, **17**, 26742680.
- [22] T. Shimada, T. Xu, Y. Araki, J. Wang, T. Kitamura, *Adv. Electron. Mater.*, 2017, **3**, 1700134.
- [23] S. Z. Bisri, S. Shimizu, M. Nakano, Y. Iwasa, *Adv. Mater.*, 2017, **29**, 1607054.

- [24] A. Lindman, P. Erhart, G. Wahnström, *Phys. Rev. B*, 2016, **94**, 075204.
- [25] G. Geneste, B. Amadon, M. Torrent, G. Dezanneau, *Phys. Rev. B*, 2017, **96**, 134123 (2017).
- [26] P. Erhart, A. Klein, D. Åberg, B. Sadigh, *Phys. Rev. B*, 2014, **90**, 035204.
- [27] S. Li, T. Birol, *Phys. Rev. Lett.*, 2021, **127**, 087601.
- [28] G. Kresse, J. Hafner, *Phys. Rev. B*, 1993, **47**, 558.
- [29] G. Kresse, J. Furthmüller, *Phys. Rev. B*, 1996, **54**, 11169.
- [30] P. E. Blöchl, *Phys. Rev. B*, 1994, **50**, 17953.
- [31] G. Kresse, D. Joubert, *Phys. Rev. B*, 1990, **59**, 1758.
- [32] O. Grotheer, C. Ederer, M. Fähnle, *Phys. Rev. B*, 2001, **63**, 100401.
- [33] J. Heyd, G. E. Scuseria, M. Ernzerhof, *J. Chem. Phys.*, 2003, **118**, 8207.
- [34] A. V. Krukau, O. A. Vydrov, A. F. Izmaylov, and G. E. Scuseria, *J. Chem. Phys.*, 2006, **125**, 224106.
- [35] A. M. Glazer, *Acta Crystallogr. B*, 1972, **28**, 3384.
- [36] A. R. Chakhmouradian, R. H. Mitchell, *J. Solid State Chem.*, 1998, **138**, 272277.
- [37] A. Krause, W. M. Weber, D. Pohl, B. Rellinghaus, A. Kersch, T. Mikolajick, *J. Phys. D: Appl. Phys.*, 2015, **48**, 415304.
- [38] T. Higuchi, T. Tsukamoto, K. Kobayashi, S. Yamaguchi, Y. Ishiwata, N. Sata, K. Hiramoto, M. Ishigame, S. Shin, *Phys. Rev. B*, 2001, **65**, 033201.
- [39] C. Hartmann, J. Laurencin, G. Geneste, *Phys. Rev. B*, 2023, **107**, 024104.
- [40] H. Kay, P. C. Bailey, *Acta Crystallogr.*, 1957, **10**, 219226.
- [41] H. Chen, N. Umezawa, *Phys. Rev. B*, 2014, **90**, 035202.
- [42] T. Xu, T. Shimada, Y. Araki, M. Mori, G. Fujimoto, J. Wang, T. Y. Zhang, T. Kitamura, *npj Comput. Mater.*, 2019, **5**, 23.
- [43] W. Zhong, R. D. King-Smith, and D. Vanderbilt, *Phys. Rev. Lett.* 1994, **72**, 3618.
- [44] M. Schie, A. Marchewka, T. Müller, R. A. D. Souza, R. Waser, *J. Phys.: Condens. Matter*, 2012, **24**, 485002.

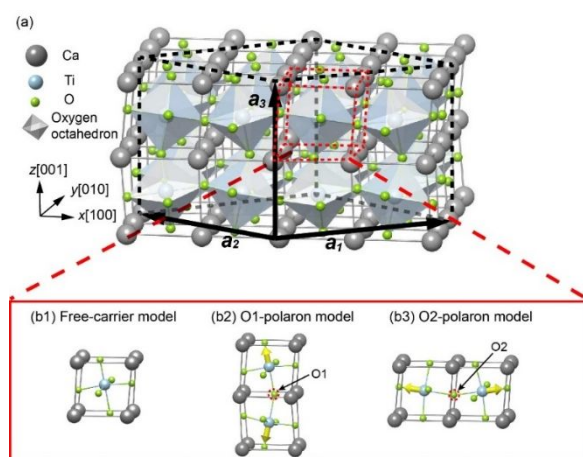


Fig. 1. (a) Simulation model of CaTiO_3 crystal with hole. The black dot box indicates the simulation supercell. a_1 , a_2 , and a_3 are cell vectors of the simulation supercell. (b1-b3) Atomic configurations for free-carrier and polaron models. Yellow arrows indicate initial small displacements of Ti atoms.

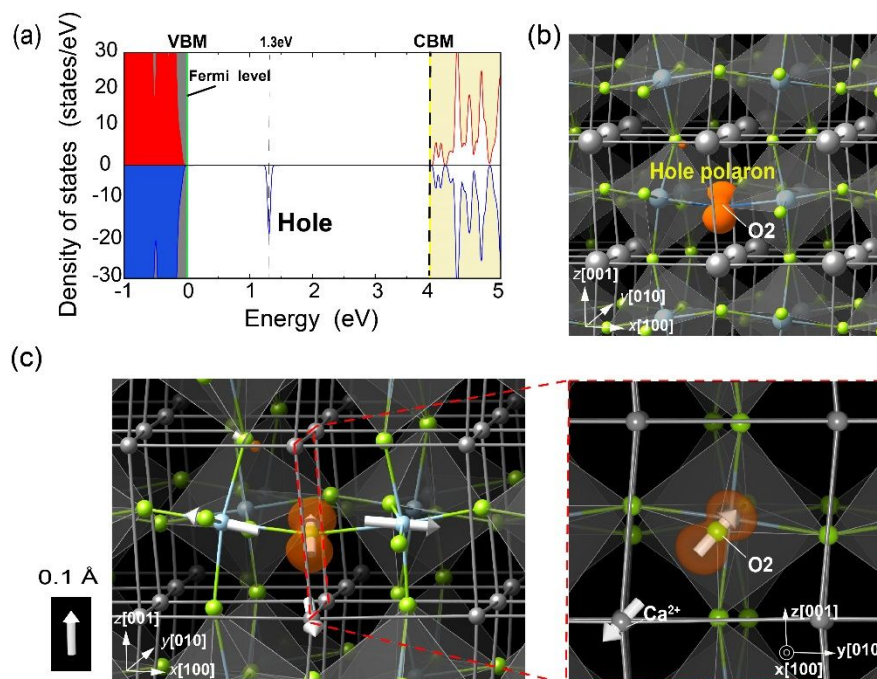


Fig. 2. (a) Density of states of the O2-Polaron in CaTiO₃. The red and blue areas (lines) indicate the occupied (unoccupied) states of up-spin and down-spin, respectively. (b) Charge density distribution of the O2-Polaron in CaTiO₃. The yellow area represents the iso-surface of charge densities of 0.02 Å⁻³. (c) The distribution of atomic displacements \mathbf{d} (white arrows) around the hole polaron in CaTiO₃.

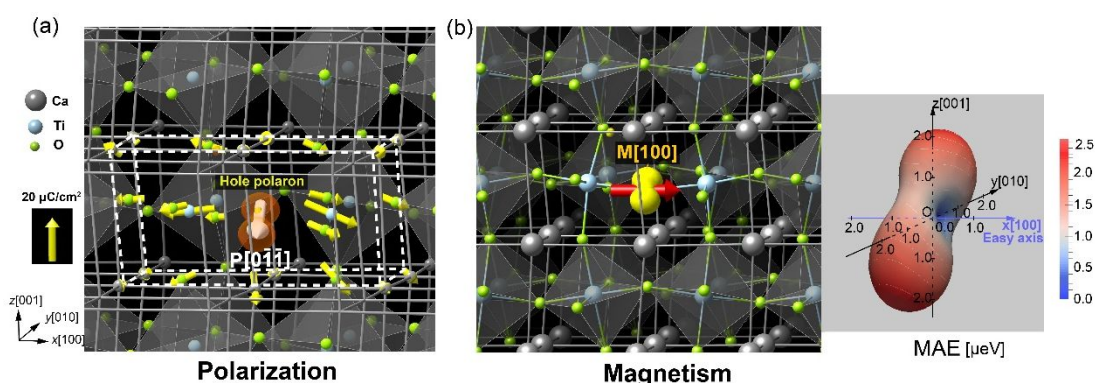


Fig. 3. Multiferroic properties of the hole polaron in CaTiO₃. (a) The distribution of polarization \mathbf{P} around the hole polaron. The yellow arrows indicate local polarization, and the white arrow indicates their average. (b) Magnetic spin-density distribution of the hole polaron, in which the yellow area represents the iso-surfaces of spin-densities of $0.10 \mu_B/\text{\AA}$, and the red arrow denotes the direction of magnetic moment of the hole polaron. The right panel shows the magnetocrystalline anisotropy energy surface of the hole polaron.

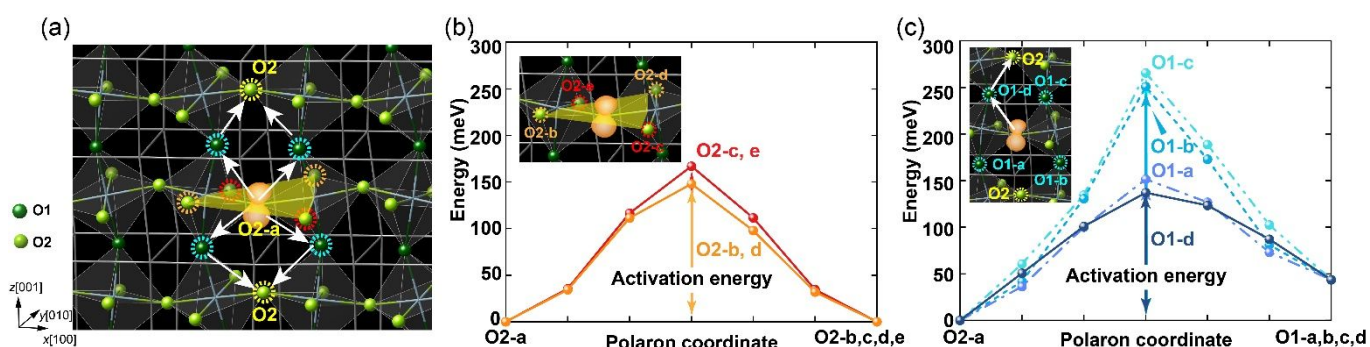


Fig. 4. (a) The eight kinds of migration pathways for the hole polaron in different O2 atoms, including (b) four (001) in-plane migration pathways (denoted by the yellow plane) and (c) four out-of-plane migrations through O1 (denoted by the white arrows).

Table 1 The polarization and magnetic moment directions for the hole polaron localized on each O2 atom. The characters p1, ..., p8 correspond to O atoms in Fig. S4(a).

O2 number	p1	p2	p3	p4
Polarization \mathbf{P}	$[0 \bar{1} \bar{1}]$	$[\bar{1} 0 1]$	$[0 1 1]$	$[1 0 \bar{1}]$
Magnetic moment \mathbf{M}	$[1 0 0]$	$[0 1 0]$	$[\bar{1} 0 0]$	$[0 \bar{1} 0]$
O2 number	p5	p6	p7	p8
Polarization \mathbf{P}	$[0 \bar{1} 1]$	$[\bar{1} 0 \bar{1}]$	$[0 1 \bar{1}]$	$[1 0 1]$
Magnetic moment \mathbf{M}	$[1 0 0]$	$[0 1 0]$	$[\bar{1} 0 0]$	$[0 \bar{1} 0]$